



**HAL**  
open science

# Multiscale roughness analysis of engineering surfaces: A comparison of methods for the investigation of functional correlations

Gaëtan Le Goïc, Maxence Bigerelle, Serge Samper, Hugues Favrelière,  
Maurice Pillet

## ► To cite this version:

Gaëtan Le Goïc, Maxence Bigerelle, Serge Samper, Hugues Favrelière, Maurice Pillet. Multi-scale roughness analysis of engineering surfaces: A comparison of methods for the investigation of functional correlations. *Mechanical Systems and Signal Processing*, 2016, 66-67, pp.437-457. 10.1016/j.ymssp.2015.05.029 . hal-01202891

**HAL Id: hal-01202891**

**<https://hal.science/hal-01202891>**

Submitted on 2 Apr 2024

**HAL** is a multi-disciplinary open access archive for the deposit and dissemination of scientific research documents, whether they are published or not. The documents may come from teaching and research institutions in France or abroad, or from public or private research centers.

L'archive ouverte pluridisciplinaire **HAL**, est destinée au dépôt et à la diffusion de documents scientifiques de niveau recherche, publiés ou non, émanant des établissements d'enseignement et de recherche français ou étrangers, des laboratoires publics ou privés.

# Multiscale roughness analysis of engineering surfaces: A comparison of methods for the investigation of functional correlations

Gaëtan Le Goïc<sup>a,b,\*</sup>, Maxence Bigerelle<sup>c</sup>, Serge Samper<sup>b</sup>, Hugues Favrelière<sup>b</sup>,  
Maurice Pillet<sup>b</sup>

<sup>a</sup> Laboratoire Electronique, Informatique et Image, LE2I UMR6306, CNRS, Arts et Métiers, Univ. Bourgogne Franche-Comté, Dijon, France

<sup>b</sup> Laboratoire Systèmes et Matériaux pour la Mécatronique, SYMME EA 4144, Université de Savoie Mont-Blanc, Annecy, France

<sup>c</sup> Laboratoire de Thermique, des Ecoulements, de Mécanique et Matériaux en Mise en Forme, TemPo/LAMIH UMR CNRS 8201, Université de Valenciennes et du Hainaut Cambresis, Valenciennes, France

---

## A B S T R A C T

This study investigates the correlations between the topography of different damaged rough surfaces and process conditions. Several surfaces are measured and compared to determine if they can be discriminated. The analysis is performed by using Gaussian Filtering, Wavelet Transform and a more recent approach named Discrete Modal Decomposition. Standardized 3D roughness parameters are computed for each multiscale method, filter (e.g., high-pass, low-pass and band-pass) and available scale. The relevance (i.e., the ability to discriminate surface topographies corresponding to different process conditions) is then investigated using a statistical analysis based on the MesRug<sup>TM</sup> expert system. The results indicate clear differences between the multiscale methods and show that the Wavelet approach is useful when characterizing localized surface defects while Gaussian Filtering is more appropriate for highly periodic morphological structures. For more complex topographies, this study also clearly shows that the Discrete Modal Decomposition exhibits compelling abilities that fall between those of the Gaussian and Wavelet approaches; this method is clearly more relevant than the Gaussian method in the case of localized defects and less relevant in the case of highly periodical structures and fractal surfaces ( $1/f^\alpha$  spectrum). This can be explained by the modulated frequency/amplitude descriptors generated via the modal basis.

### Keywords:

Roughness analysis  
3D topography  
Discrete Modal Decomposition  
Gaussian Filtering  
Discrete Wavelet Transform

---

## 1. Introduction

Many surface roughness parameters can currently be used to characterize the relationship between the surface roughness and its behaviour. The evolution of surface measuring machines has enriched the historical 2D parameters [1–3] by adding 3D parameters [4,3] that notably include the ability to better estimate anisotropy. A recurrent issue in functional surface roughness analysis is the ability to determine the relevant parameter(s) with respect to the function studied. The calculation of these roughness parameters also requires low-frequency components filtering (i.e., primary form and waviness). The filtering method choice and the appreciation of the threshold that limits the primary form, waviness,

roughness and even micro-roughness are often arbitrary and influence the results. The use of a Multiscale Analysis (MA) method provides a more generic approach to this issue, but determining which method, surface parameter, and analysis scale is relevant with respect to an analysed function is still difficult. This paper aims to propose a statistical response to this issue and improve the effectiveness of functional surface topography analysis in tribology.

Three currently available multiscale techniques are compared in this study (Section 2). These techniques are the Gaussian Filtering (GF), the Discrete Wavelet Transform (DWT) and a more recent technique named Discrete Modal Decomposition (DMD). The statistical analysis is performed using the MesRug™ expert system (Section 4), which enables a generic calculation of the relevance indicators for each set of surface parameter, method, filter, and analysis scale. To ensure representative results, a large collection of surface measurements extracted from different tribological processes (Section 2) are analysed, and results are finally presented and synthesized in Section 5.

## 2. Spectrum of the study

If surfaces and interfaces roughness analysis are of major interest to study and characterize many functions, the case of vibration phenomena during sliding contact is particularly interesting. For example, the roughness components of total hip implant interfaces induce friction that may be materialized by squeaking [5]. In other cases, an ideal fluid film lubrication regime is sought to minimize the produced vibration; an increased roughness on damaged surfaces can lead to a change in the lubrication regime [6–8]. Another vibration phenomena induced by roughness components is adhesion: Bengisu and Akay [9] have shown that the stick-slip model sums adhesive and deformation forces over all asperities and that the phenomenon was directly linked to roughness slope indicators. In the same way, abrasion modifies the surface morphology [10] and involves a change of vibration characteristics during a sliding process; wheel-raise noise in grinding processes is generally thought to be wheel and rail structural vibrations excited by a combination of the wheel and rail surface roughness components [11]; roller bearing vibrations are induced by excitations from surface waviness and roughness components through a lubricating film [12–14]; during rolling processes (i.e., vibration of the rolling mill structure), a non-steady-state lubrication and friction during rolling involves a change of roughness [15]; in a turning process, the choice of optimized cutting parameters is essential to control the required surface quality, and the difference between real and specified surface roughness is often caused by the influence of dynamic phenomena, such as a built-up edge, the friction of cut surface against tool point and other vibrations [16–18].

As roughness analysis often yields to a better understanding and control of the state of vibration during sliding contact on damaged surfaces, the spectrum of this study was composed by various sliding contact functions of those mentioned below. Each process/function is analysed within two classes of parameters, identified by A and B. Experiments are presented in Table 1, and a brief description of surface processes/function and measuring parameters is presented for each case study. If not mentioned, measurements are made by means of a White Light Interferometer (WLI) Zygo NewView 7300 equipped with a high-speed camera at 320 × 240 pixels with a 20 × Mirau objective lens. The working distance is 4.70 mm, the optical resolution is 0.71 μm and the spatial sampling is 1.09 μm for both X- and Y-axes. To obtain reliable statistical estimation, up to 20 elementary surfaces are measured and stitched together with an overlap of 20% to obtain measurements across surfaces with dimensions of 1.19 × 0.89 mm. The multi-scale techniques (i.e., GF, DWT and DMD) used in this paper are presented in Section 3.

### 2.1. Sendzimir cold rolling process

The studied rolling process is used to reduce an austenitic stainless steel strip from 3 to 0.49 mm. The rolling mill is a Sendzimir stand made up of 2 work rolls with diameters below 100 mm that rotate at between 300 and 650 rev/min. During the process, the rolls maintain pressure on the strip to reduce its thickness. The final thickness is obtained after 10 rolling passes, reducing the ratio from 25% to 10%. The roughness gradient between the sheet and blasted cylinder is important. Large crushing asperities occur but are constrained by the trapping of lubricant in the valleys. As the first three rolling passes are critical in the scrub of surface flaws, two specimens are extracted from the industrial process to be analysed, after 1 and 3 passes (Groups A and B, respectively). 700 × 525 μm measurements are obtained for each group.

**Table 1**  
Surface processes/functions and associated case study.

Process/function	Study	Process/function	Study
Cold rolling	Influence of number of passes	Tribo corrosion	Wear on knee prosthesis
Moderate impact	Sand blasting	Plastic deformation	Cold rolling surfaces
Abrasion	Polishing surfaces	Adhesion	Adhesion on a molding process
Tribometer	Study with different lubricant	Surface polishing	Brushing
Super finishing	Belt finishing process	High impact	Shot peening
Low impact	Super finishing by ultrasonic sand blasting	Fatigue contact	fatigue with different lubricants
Tooled surface	Analyses of high precision turning	Grinding	Super finishing by grinding process

## 2.2. Sandblasting process

The effect of the working pressure on the sandblasted surface morphology is investigated by comparing the resulting topographies after 1 and 3 bar pressures have been applied (Groups A and B, respectively), and by fixing the angle at 90°, the distance at 5 cm and the duration at 60 s of the shooting process.

## 2.3. Polishing process

The samples are cut from a 30-mm-diameter cylinder of TiAl<sub>6</sub>V<sub>4</sub> alloy (20-mm height). The chemical composition (% weight) of the specimens is Al (6.13), V (4.00), Fe (0.11), O (0.11), C (0.004), N (0.006), Y (< 0.001), H (0.0007) and Ti (base). A specific automatic Struers® polishing machine that has a dual off-centre rotating movement is used for the experiments. Eleven different abrasive papers of silicon carbide grain have been used with grain sizes from 200 µm to 5 µm. Each grinding step is performed with a new silicon carbide paper under a fixed load and time (150N, 3 min) and using the same conditions of water lubrication (5 rev s). For this study, the grits used for comparison are 120 and 220 µm (i.e., Groups A and B, respectively).

## 2.4. Bi-disk tribometer process

For this process, the study aims to compare the effects of two different lubricants on a bi-disk tribometer: oil A is known to not produce micro-pitting on the surface, while oil B produce micro-pitting. The experiment is performed over 42 h with 2 convex and cylindrical disks that produce elliptic contact. The disks are made of the same steel material (16MnCr5) and are mounted on brooches that are individually driven at a maximum speed of 10,500 rpm. A constant normal load is applied, and tangential force is monitored in real-time during the experiment. Measurements of 0.9 × 1.3 mm are performed for each group with a Bruker NT Interferometer.

## 2.5. Belt finishing process

The grinding belt process consists of applying an abrasive oscillating belt of low thickness on a rotating manufactured specimen. To ensure the reproducibility of the process, five inner ball bearings are tooled for each test conditions. The experiment is conducted using two specimens that were turned and rectified. All samples are then manufactured with the same lubrication conditions: 1 bar of contact pressure and a belt feed speed of 100 mm/min. The belt width is 20 mm. Tagushi's experimental design is used to evaluate the effects of the belt grinding process conditions on the resulting roughness, using the two sets of parameters detailed in Table 2.

## 2.6. Hot mill rolling

Roll wear is a process where mechanical and thermal fatigue combines with impact, abrasion, adhesion and corrosion, which all depend on system interactions rather than material characteristics. This study consists of analysing wear along the roll. Group A measurements are close to the sample centre while Group B are 1.30 m distant.

## 2.7. Ultrasonic shot peening

To study ultrasonic shot peening, surfaces of AISI 316L stainless steel are first carefully polished and then ultrasonically shot peened. The analysed functional parameter is coverage (Group A: 100%, Group B: 1%). For both groups, the shot is made of 100C6 steel balls with a diameter of 2 mm with a 60 µm sonotrode vibration amplitude. 20 measurements from each group are analysed.

## 2.8. Precision Hard Turning

The influence of feed rate (Group A: 50 µm/rev, Group B: 200 µm/rev) on Precision Hard Turning (PHT) is analysed. This process offers substantial benefits to grinding: it is environmentally friendly, flexible and cost-effective. It also induces deep compressive residual stresses, which increase fatigue life. The surface quality obtained using PHT is a criterion for surface integrity and plays an important role in terms of surface functionality. For this experiment, 100Cr6 bearing steel (AISI 52100) heat-treated to an average

**Table 2**  
2 Belt finished groups process parameters.

Group	A	B
Contact wheel hardness	hard	soft
Belt grit size (µm)	9	40
Work piece rotation speed (rpm)	500	100
Cycle time (s)	9	3
Axial oscillation frequency (Hz)	10	1.6

hardness of 611 HRC was used as the work piece material (diam.=70 mm, length of cut=14 mm). Cutting tool inserts were mounted at a rake angle of  $\gamma_0 = -6^\circ$ , an inclination angle of  $\lambda_s = -6^\circ$ , a cutting edge angle of  $\chi_r = 95^\circ$ , a clearance angle of  $\alpha = 0^\circ$ , and a nose radius  $r=0.8$  mm. Experiments are made with 210 m/min cutting speed, and a 5  $\mu$ m depth of cut.

### 2.9. Wear of knee prosthesis

Wear of Ultra-High Molecular Weight Poly-ethylene (UHMWPE) is a major factor affecting the longevity of total knee prostheses. Wear debris released by the tibia component can illicit biological responses and cause periprosthetic osteolysis, which leads to alteration of prostheses. Femoral and tibia components prostheses materials are CrCo and UHMWPE. The prosthetic parts in contact with the resected parts of the bone are constituted by a multitude of small balls to allow the reconstitution process. Surface topography is investigated to understand UHMWPE wear mechanisms. Measurements are made with contact and interferometric profilometry. Two different types of scratches are observed; large scratches (200  $\mu$ m) are caused by balls that have migrated from both the bone femoral and tibia interfaces to the prostheses joint space, and participate in abrasive third-body wear of the polyethylene component; small scratches (less than 25  $\mu$ m) are produced by abrasion with third bodies composed of polyethylene (Fig. 1).

### 2.10. Plastic deformation (roping)

Austenitic steels can both produce orange peel and anisotropic surface morphology defects. Orange peel defects result on slip planes within a grain disrupting the surface and can be prevented by maintaining a small grain size. Anisotropy, which is less severe, can cause earing in which round blanks deform non-uniformly, causing excess ear-shaped material to extend beyond the intended dimensions of the component. Ferritic stained steels can also present a more specific surface defect called roping. Two classes of defects are identified via visual inspection: small (Group A) and higher ripping effect (Group B). 20 measurements from each group are analysed.

### 2.11. Lipstick morphology during moulding

Lipstick is made of dyes and pigments in a fragranced oil-wax base, and the manufacturing process consists of two separate steps: melting and mixing the lipstick, and pouring the mixture into the tube. The lipstick is ready to be poured into the tube when the lipstick mass is mixed and free of air. The melted mass is dispensed into a mould, which consists of the bottom portion of an elastomer tube and a shaping portion that fits snugly with the tube. Two moulds are obtained with different elastomers: one produces bright lipstick (Group A) while the other produces a lipstick with lower gloss (Group B). Measurements are conducted with a WLI (Veeco NT 1500). Stitched images are produced from up to 125 0.15  $\times$  0.12 mm images (Table 3).

### 2.12. Brushing super finishing process

A superfinition operation is based on a duplex treatment: a short shot peening is firstly processed at two different pressures, and then abrasive-assisted brushing is used to debur the parts. The deburring rate during the abrasive brushing, the work piece material, the abrasive grit size, and the type and rotational speed of the brush are kept constant. The brightness of the two samples are shown to vary: samples of Group A are twice as bright as samples from Group B. Measurements are made with a WLI (Veeco NT 1500). A stitched measurement is built from up to 125 0.15 mm  $\times$  0.12 mm individual measurements.

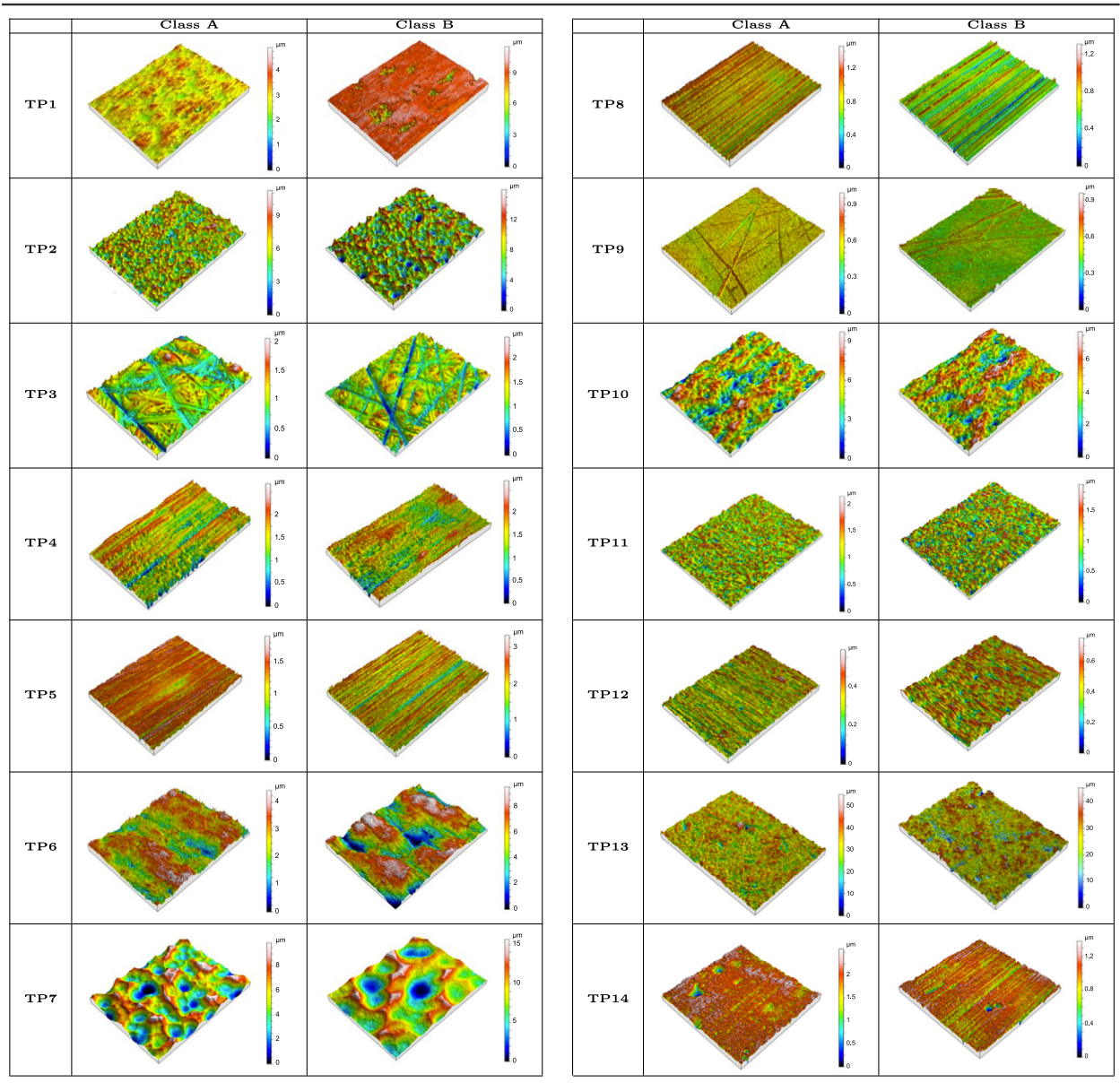
### 2.13. Ball bearing process

The effect of the coverage rate on a ball bearing process is analysed (Group A: 100%, Group B: 200%). Samples are cut from a 20 mm rod of AISI 316L steel into 15 mm thick discs and are shot peened at 20–30 Almen intensity. 3D roughness measurements are made with a white light Interferometer (Veeco NT 1500). Stitched images are obtained with 4 1.4  $\times$  1.4 mm individual acquisitions.



Fig. 1. The 2 wear zones of analysis.

**Table 3**  
Measurement samples for tribological processes/functions TP1-14.



#### 2.14. Contact fatigue of gears with two lubricants

Contact fatigue performance is defined by the interaction of material shear fatigue strength and the applied subsurface shear stress profile. Two experiments are performed on a 16MnCr5 steel initially polished with two lubricants (i.e., Groups A and B). The duration of the experiments is 500 h. Measurements are performed with a Bruker NT Interferometer on a  $0.7 \times 0.3$  mm area centred on the wear track.

### 3. Methods: multiscale filtering and analysis

The notion of scale is essential in surface metrology. A first separation involves isolating three frequency or wavelength ranges. Lower frequencies refer to the primary form, while higher frequencies correspond to roughness, which is composed of pseudo-periodic components and chaotic components that are discontinuous; this is called micro-roughness. Waviness refers to the medium frequency components, which lie between the form and roughness frequencies. Fig. 2 illustrates this

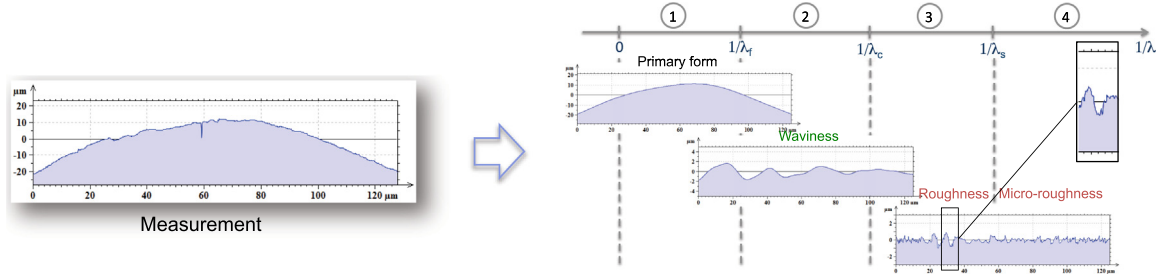


Fig. 2. Separation of roughness, waviness and primary form.

separation on a surface extracted profile. If this separation in the three ranges of variation is sufficient to correlate with the analysed behaviour in some simple cases, Raja and Radhakrishan [19] show that both the need for manufacturers to control their surface finishing process and the need in functional analysis require finer frequency analysis on the entire range of wavelengths available from the measurements. The so-called multi-scale and/or multi-resolution methods include the ability to address this issue [20,21], application examples to abrasion and friction are detailed respectively in [22] and [23].

Historically, the method used to filter and/or separate surface measurements geometric variations in surface metrology was the analogue RC or 2RC filter, which has now largely been replaced by Gaussian Filtering (GF). In 2000, in their paper on quantitative characterization, De Chiffre et al. [24] describe changing uses in surface metrology and filtering, and particularly the fractal analysis and area-scale methods [25,26], the motifs method [27] and the discrete wavelet transform (DWT). This non-exhaustive list can be completed by morphological filtering [28,29], and, more recently, a multiscale decomposition method based on descriptors derived from dynamics called Discrete Modal Decomposition (DMD) has also been implemented [30].

It emerges that, both in number and typology, the variety of available multiscale methods often yields an arbitrary choice for tribologists. Thus, this comparison study aims to propose an objective methodology and criteria when performing a multiscale topography functional analysis. This methodology is generic and can be applied to any multiscale approach; however, this study focuses on GF, DWT, and DMD approaches.

### 3.1. Fourier transform and Gaussian Filtering

The Fourier transform is a generalization of the Fourier series to a non-periodic case. It enables decomposition in one or two dimensions (i.e., profile or area). The decomposition is made in a vector basis constructed from harmonic sines and cosines. In the context of industrial surfaces, Raja [31] applied this method onto roughness profiles while Peng and Kirk [32] show that a Fourier transform in two dimensions can effectively characterize the texture of a surface and particularly its isotropy or anisotropy. The use of the Fourier transform is well known in texture surface analysis or profile analysis, including its use in characterizing form components. As an example, standard ISO-12781-2 [33] refers to parameters involving harmonic components of the discrete Fourier transform to evaluate flatness. The Gaussian filter is also currently normalized for the calculation of roughness and waviness parameters [3] and is based on a Gaussian weighting function, a cut-off wavelength (cut-off), and a percentage of 50% attenuation. As an example, the weighting and the transfer functions of a Gaussian low-pass filter are given by the following equation (from [19]):

$$S(x) = \frac{1}{\alpha\lambda_c} \exp\left[-\pi\left(\frac{x}{\alpha\lambda_c}\right)^2\right]; \quad \frac{A_{output}}{A_{input}} = \exp\left(\pi\left(\alpha\frac{\lambda_c}{\lambda}\right)^2\right) \quad \text{with } \alpha = \sqrt{\ln 2/\pi} \quad (1)$$

Thus, for a signal  $V(x)$ , the roughness profile  $R(x)$  is obtained by the following operation:

$$R(x) = V(x) - V(x) * S(x) \quad (\text{where } (*) \text{ represents the convolution product}) \quad (2)$$

### 3.2. Discrete Wavelet Transform (DWT)

This multi-resolution approach enables the decomposition of a surface at different scales [34], yielding its metrological characteristics in terms of wavelength and phase [35]. The work of Chen et al. on industrial surfaces [20,36] demonstrates that this method links aspects of machining and the function of surfaces with multi-scale features. In the field of tribology, Lee et al. [37] applied wavelet decomposition to roughness profiles and showed that this filtering method can also be well suited for metrological applications. More recently, Rosenboom et al. [38] demonstrated the benefits of the DWT in detecting defects on an industrial local area. A large selection of localized waveforms can be employed as long as they satisfy predefined mathematical criterion. The wavelet (see Fig. 3) selected for this study is the wavelet *coiflet* (degree 2). Continuous wavelet transform (CWT) [39,40] is an evolution wavelet analysis that differs from DWT by the use of a variable window width, which is related to the scale of observation. This enables the isolation of higher frequency features, and

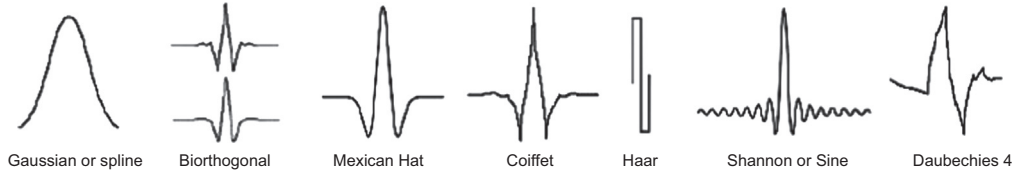


Fig. 3. Different wavelets.

allows the method to be more adaptive. The wavelet transform of a signal  $V(x)$  is defined as

$$T(a, b) = \frac{1}{\sqrt{a}} \int_{-\infty}^{+\infty} V(x) \psi^* \left( \frac{x-b}{a} \right) dx \quad \text{with} \quad \begin{cases} \psi^*(x): & \text{complex conjugate of } \psi(x) \\ a: & \text{dilation parameter} \\ b: & \text{location parameter} \end{cases} \quad (3)$$

### 3.3. Discrete Modal Decomposition (DMD)

A Discrete Modal Decomposition decomposes a signal within a spectral basis built from eigenmodes. Similar to the Discrete Fourier or Cosinus Transform (DCT) [41], this projection method projects the measured surface into an eigen-basis built from structural dynamics. This eigen-basis is defined by its eigenvectors, called modal vectors, and gives the method its name. The modal basis derives from the resolution of the classical dynamic equation:

$$M \cdot \ddot{q} + K \cdot q = 0 \quad \text{with} \quad q = q(x, y, t) = \sum_{i=1}^{+\infty} Q_i(x, y) \cdot \cos(\omega_i t) \quad (4)$$

where  $M$  and  $K$  stand for the mass and the stiffness matrices, respectively, and  $q(x, y, t)$  stands for the displacements, which characterizes the modal shapes.

The decomposition operation is carried by projecting the measured surface onto the free-form surface family composed by the structure eigenmodes (Fig. 4a). Projected surfaces can thus be expressed as the sum of a linear combination of the modal vectors and the decomposition residual (Eq. (5)). Projection results can be shown in the form of a modal spectrum of amplitudes. An example of DMD projection is presented in Fig. 4b:

$$V = \sum_{i=1}^{N_q} \lambda_i Q_i + \epsilon(N_q) \quad \text{with} \quad \begin{cases} Q_i: & \text{modal vectors composing the modal basis} \\ \lambda_i & \text{modal coordinates} \\ N_q: & \text{number of modes of decomposition} \end{cases} \quad (5)$$

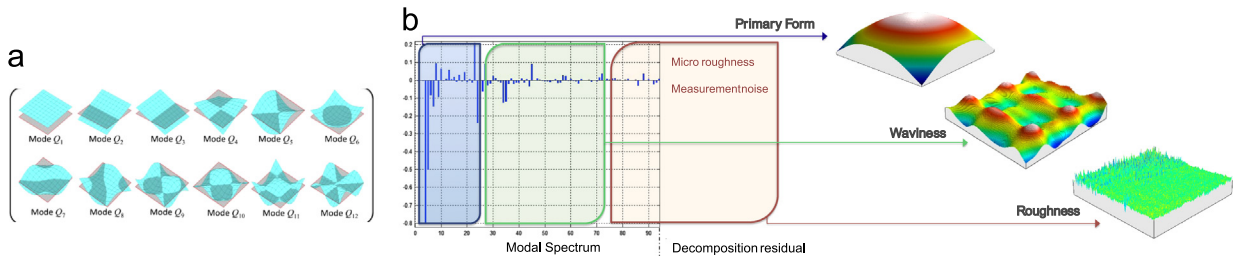


Fig. 4. (a) First modes of the DMD free-form surface family of projection. (b) DMD projection: modal spectrum and filtering principle.

DMD can be used to describe many types of geometries (i.e., profiles or surfaces). Initially implemented to characterize primary form variations [30,42], this method has been generalized to waviness and roughness by varying the width of the analysis window [43,5]. As an illustration, Fig. 5 shows high-pass and low-pass components resulting from the application of the DMD on a surface extracted from hot rolling mill group (see Section 2.6).

## 4. Comparison methodology: Implementation and method

In this section, we present the detailed application of the proposed method on surfaces obtained by cold rolling process as an example (see Section 2.1). This study consists of four main steps, which are detailed below:

- (i) Samples extraction and measurement.



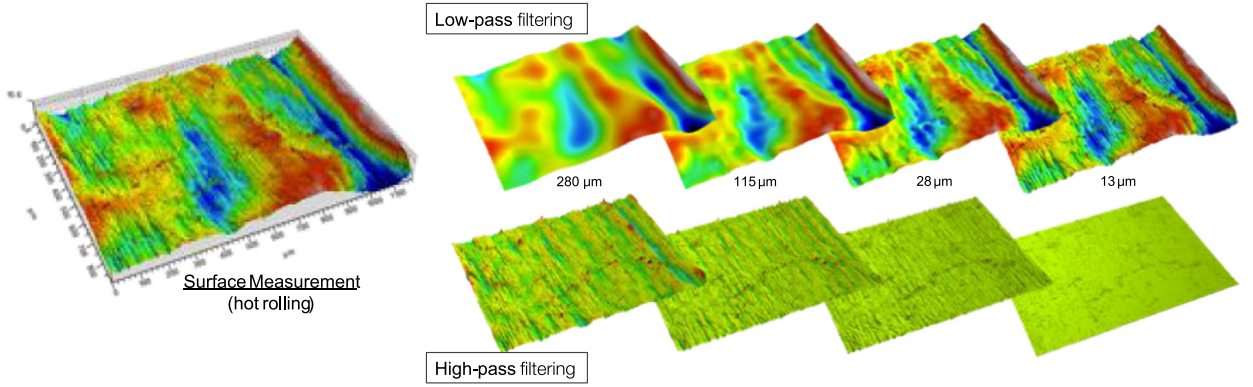


Fig. 5. Multiscale DMD applied on a hot mill rolled sample.

- (ii) Multiscale decompositions using the 3 approaches.
- (iii) Computing roughness parameters.
- (iv) Statistical analysis and interpretation.

(i) *Samples extraction and measurement*: Tribological processes/functions have been described previously in Section 2. The process chosen to illustrate this section is cold rolling, and the two groups of 30 extracted surfaces correspond to one (Group A) and three rolling passes (Group B).  $700 \times 525 \mu\text{m}$  surfaces have been measured by means of a WLI ( $0.55 \mu\text{m}$  spatial sampling).

(ii) *Multiscale decomposition using the three selected approaches*: The three multiscale methods (see Section 3) are applied to each measured sample and processed for each method (e.g., high pass and low pass filtering, detailed reconstruction for the wavelet transform). Thus, a total of approximately 6500 surfaces are generated to analyse the process/function, corresponding to the filtered components obtained by using the decomposition methods and varying the analysis scale.

(iii) *Computing roughness parameters*: For each generated surface, roughness parameters are calculated to apply the expert system MesRug<sup>TM</sup> on the data and to determine each parameter/scale relevance. The obtained relevance value is linked with the ability to discriminate the two groups of surfaces by using the parameter considered. Most parameters from ISO 25178 and EUR 15178N are systematically processed. In addition, other more specific parameters have also been computed, as the density, the mean and the maximum depth of furrows ( $Dens\_plis$ ,  $P\_moy\_plis$  and  $P\_max\_plis$ ), the roughness amplitude and mean height ( $Amp$  and  $Hmoy$ ), and the number of 3D-Motifs [44] ( $nb_{motifs}$ ).

(iv) *Statistical analysis and interpretation*: To evaluate the relevance of roughness parameters computed at certain spatial scales, an appropriate statistical tool should be used in the sequence. The most relevant scale is investigated by variance analysis, which is essentially an implementation of the generalized linear model. The formula is as follows:

$$p_i(F, T, \varepsilon, j, n_j) = \alpha_0 + \alpha_j(i, F, T, \varepsilon) + \xi_j(i, F, T, \varepsilon, n_j) \quad (6)$$

- $p_i(F, T, \varepsilon, j, n_j)$  is the value of the  $i$ -th roughness parameter computed on the  $n$ -th surface of group  $j$  (i.e., A or B) using the multiscale method  $F$  (i.e., modal, wavelet or Gaussian), the filter  $T$  (i.e., pass band, low pass, high pass), and the evaluation length  $\varepsilon$  (i.e., scale).
- $\alpha_j(i, F, T, \varepsilon)$  represents the influence on the  $i$ -th roughness parameter (using  $F$ ,  $T$  and  $\varepsilon$ ) of the process condition  $j$  (i.e., A or B).
- $\xi_j(i, F, T, \varepsilon, n_j)$  is a zero-mean Gaussian noise with standard deviation.

For each roughness parameter computed with all combinations of  $F$ ,  $T$  and  $\varepsilon$ , values are calculated by the least square method. From these values, between- and within-group variabilities (i.e., estimation errors of the roughness parameter for each group) are obtained, and the result  $F_{i,F,T}(\varepsilon)$  is the ratio between these two values.  $F$  indicates the effect of class A or B on the roughness parameter's value with its estimation error. Consequently, a value of  $F_{i,F,T}(\varepsilon)$  near to 1 indicates a negligible roughness parameter  $P_i(F, T, \varepsilon)$  estimated at the evaluation length  $\varepsilon$  to differentiate the two groups of surfaces; the higher the value of  $F_{i,F,T}(\varepsilon)$  is, the more relevant the parameter  $P_i(F, T, \varepsilon)$  is [45]. Then, both  $F_{i,F,T}(\varepsilon)$  and the chosen roughness parameter are compared with regard to scale. The highest value of  $F_{i,F,T}(\varepsilon)$  represents the most relevant roughness parameter, as calculated with  $F$ ,  $T$  and  $\varepsilon$ , to discriminate the two groups A and B. Thus, a relevance classification based on  $F$ -values can be performed in descending order.

To improve the robustness of the  $F$  relevance indicator, a bootstrap technique is performed. This resampling technique estimates the coefficients' statistical modelling error in the computation to create a new dataset by randomly sampling with replacement from the original data set; then, the same statistical analysis as was carried out on the original data set is

performed on the new data set [46]. Applied to the analysis of variance, this technique obtains the variability of  $F_{i,F,T}(\epsilon)$  [47]. Bootstrapping is also used to estimate the error of the mean roughness parameters, called  $\bar{p}_{i,k}(F, T, \epsilon, j, n_j)$ , where  $k$  denotes the bootstrap number [48].

Results for Tribological Process 1 (TP1) are synthesized in Table 4. The main plot represents  $F_{i,F,T}(\epsilon)$  in decreasing order, as explained before. TP1 reveals that the most relevant parameter to discriminate groups A and B is  $V_m$  (i.e., material volume), which is calculated using the DMD method ( $F$ ), high pass filtering ( $T$ ) with an evaluation length of  $8 \mu\text{m}$  ( $\epsilon$ ). To provide a more detailed assessment of the three multiscale methods, a statistical method of classification is proposed. The 3 histograms of  $F_{i,F,T}(\epsilon)$  for the 3 methods  $F$  and 1000 bootstraps are plotted in Table 4b (i.e.,  $F_{i,Wavelet,T}(\epsilon)$ ,  $F_{i,Gaussian,T}(\epsilon)$  and  $F_{i,Modal,T}(\epsilon)$ ). However, the number of configurations can differ from one method to another; to allow a meaningful comparison, histograms are normalized and values of  $F_{i,F,T}(\epsilon)$  that are considered irrelevant using bootstrap confidence intervals are suppressed. Two main graphical interpretations can then be performed:

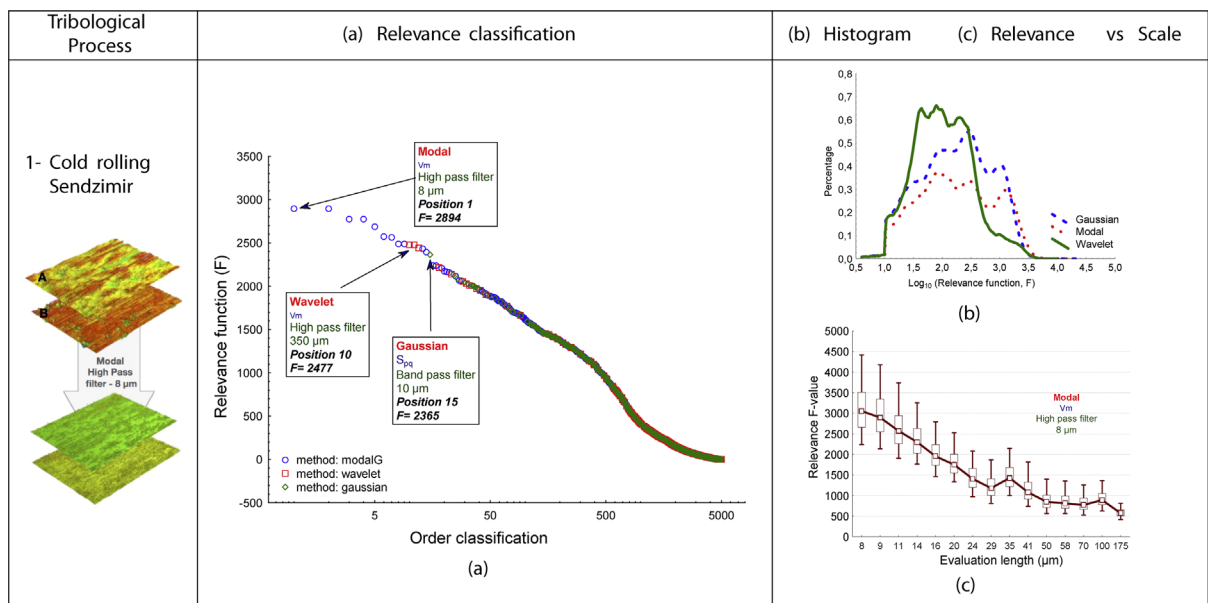
- If the histogram right tail is shown to be more important for a multiscale method, then the method is deemed more relevant.
- If the histogram area is shown to be less important for a multiscale method, the method is globally less relevant.

For TP1 (i.e., cold rolling), the lower histogram area is shown to correspond with the DMD technique. This means that globally, for this process, DMD appears less relevant than GF and WT: by selecting a roughness parameter at random, the probability of selecting a more relevant parameter is higher when using Wavelet. However, Modal and Gaussian methods present a large tail for high-value  $F$  functions (i.e., the right tail of histogram). This clearly shows that by selecting adequate relevance parameters with an appropriate evaluation length end filter  $T$ , Gaussian and Modal techniques are clearly more relevant than Wavelet Transforms. It is also shown that the relevance scale for the most relevant parameter (i.e.,  $V_m$ ) is approximately  $8 \mu\text{m}$  (Table 4c). In addition, it can be observed that the  $V_m$  associate  $F$ -value is very high ( $\approx 3000$ ), which reveals that this parameter discriminates the studied groups with a high confidence level.

## 5. Results and discussion

The methodology presented for TP1 is applied to each tribological process of the study (see Section 2). For this process (i.e., cold rolling), the  $V_m$  parameter represents the material volume at 10%. When the number of rolling passes is increased from 1 to 3,  $V_m$  increases but is localized to micro-roughness (i.e.,  $10 \mu\text{m}$ ); void volume also tends to increase. During the different passes, the lubricant slowly flows from valley to valley due to a sparse pit network. For the 13 other processes, the corresponding relevance result tables are provided in Appendix A. The functional interpretation that emerges from the relevance analysis applied to these processes is as follows:

**Table 4**  
Tribological process 1 – relevance comparison of the multiscale approaches.



**Sandblasting:** The inverse areal material ratio is the height at which a given areal material ratio of 0.1 is satisfied. For the same  $S_{mc}$ , increasing pressure increases the size of the indentation. The Band-pass filter is localized to the mean size of the ball impact (65  $\mu\text{m}$ ), and the MA thus reveals the morphology at the impact scale.

**Polishing:** The  $S_{r1}$  parameter can effectively analyse the regime of peaks. For small analysis scales, a higher  $S_{r1}$  for grade 220 than 120 characterizes micro-abrasion into grooves with a third body that presents more peaks at smaller grit sizes. For higher scales, the analysis reveals that higher grit sizes produce higher peak regimes due to ploughing and cutting.

**Bi-disk tribometer:**  $S_{vi}$  characterizes the valley fluid retention index (i.e., the ratio of the void volume at the valley zone over the RMS deviation). A large  $S_{vi}$  indicates good fluid retention in the valley zone. It appears that the B lubricant is less appropriate than A, due to a lower retention at the 90  $\mu\text{m}$  scale (i.e., pitting).

**Belt finishing:** At the 100  $\mu\text{m}$  scale, the skewness of the surface differentiates the morphology. In this analysis, it appears that samples B are clearly more eroded by the super finishing process (erosion of the existing peaks due to the previous process operation).

**Hot mill rolling:** The oxidation of carbides due to thermal conduction in the cylinder is more pronounced at the centre than at the extremities of cylinder. Large stripes induced by edge rolling are characterized by a higher  $S_{pc}$  (i.e., density of peaks) at large scales (i.e., higher than 300  $\mu\text{m}$ ).

**Ultrasonic shot peening:** The  $V_{mc}$  parameter at the 20- $\mu\text{m}$  scale can discriminate between the two groups: increasing the number of shots increases the core of the roughness given by the impact contour.

**PHT:** The density of furrows, which characterizes the number of grooves due to machining, is more pronounced on B samples due to cutting conditions.

**Wear on knee prosthesis:** Two scales must be observed: 2  $\mu\text{m}$  (i.e., nano roughness) and 50  $\mu\text{m}$  (i.e., scratches, third body abrasion). Samples B present deeper grooves, which decrease  $S_{sk}$ , even if samples of B are less damaged at smaller scales (i.e.,  $S_{sk}$  is near zero).

**Roping:** For scales near 240  $\mu\text{m}$ , the volume of voids in the core characterizes the roping effect: the higher the roping, the more important the grain displacements are. These collaborative displacements increase the volume of voids in the material.

**Lipstick:** For all scales, the density of furrows increases due to different moulding conditions, which indicates a loss of gloss of the lipstick.

**Brushing:** The density of peaks is more pronounced for samples of B. Analysing scales higher than 17  $\mu\text{m}$  identifies the signature of the previous process (i.e., sandblasting) before brushing.

**Ball bearing:** The ball bearing conditions change the density of furrows at the 40- $\mu\text{m}$  scale without considering micro-roughness.

**Gear:** Lubricant A yields an increase of the motif of waviness due to an increase in roughness.

## 5.1. Multiscale methods comparison results

Table 5 presents a synthesis of the results obtained in this study. For each MA method, an interpretation is proposed, and relevance with respect to the tribological process analysed is investigated (Section 5.1.1). A more general interpretation about such an approach (i.e., the interest of MA, the general results of the multiscale methods comparison) is also presented at the end of this section (see Section 5.1.3).

### 5.1.1. Discrete Wavelet Transform

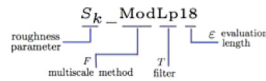
Starting with the wavelet multiscale technique, its first result confirms of the relevance of DWT when characterizing local heterogeneous morphology, such as pitting. Experiments 14 (i.e., contact fatigue of gears) and 4 (i.e., bi-disk tribometer) emphasize the wavelet approach with, respective mean orders of 956 (with respect to 2418 for Gaussian and 1113 for Modal) and 982 (1342 and 2450). Because pitting (experiment 4) can be seen as a localized tribological process [49], this study confirms the trend of the wavelet approach to be relevant to characterize tribological defaults masked into the topography as pitting roughness. Lee et al. [37] show that the main advantages of the wavelet technique over the other existing techniques is linked to its space frequency localization, and the ability to detect roughness singularities and motif size on engineered surfaces [50]. The relevant scales obtained are 80  $\mu\text{m}$  (exp. 4) 50  $\mu\text{m}$  (exp. 14), i.e., typical scales for a pit or group of pits' widths in gears [51], fretting, wear-corrosion, tribocorrosion, sliding friction [52], or pure corrosion [53]. For both processes 14 and 4, these "thin" relevant scales determine that a MA is required to improve the performance with a global filtering approach. It also shows that the analysis of roughness morphologies containing pitting at large scales is not appropriate. Concerning others processes/functions (*c.f.* details in Appendix A), it emerges that

- For pure abrasion (experiment 3), DWT appears to be irrelevant in this study. This result is confirmed in [54]. However, more investigation should be conducted to verify the influence of the use of different wavelets (type of wavelet, Discrete vs continuous wavelet transform) on relevance values.
- Wavelets appear similar in performance with respect to the other compared methods for processes 9 (wear of

**Table 5**  
results synthesis.

TP	(Rank) Identifier	F value	% Relevant	F value: mean( $\sigma$ )	TP	(Rank) Identifier	F value	% Relevant	F value: mean( $\sigma$ )
<b>1</b>	(15) $S_{pq}$ -GauDe10	2365	92.87	344(13)	<b>8</b>	<b>(1) DensPlis_GauHp27</b>	<b>4982</b>	<b>84.00</b>	<b>312(29)</b>
	<b>(1) <math>V_m</math>-ModHp8</b>	<b>2894</b>	<b>93.25</b>	<b>409(22)</b>		(9) $DensPlis\_ModHp43$	1928	80.30	177(10)
	(10) $V_m$ -WavHp350	2477	92.05	193(14)		(3) $S_{ai}$ -WavDe156	2753	81.80	204.6(18)
<b>2</b>	<b>(1) <math>S_{mc}</math>-GauDe65</b>	<b>6779</b>	<b>64.70</b>	<b>457(16)</b>	<b>9</b>	<b>(1) <math>S_{sk}</math>-GauDe2</b>	<b>283</b>	<b>56.80</b>	<b>6.4(0.6)</b>
	(36) $S_k$ -ModLp18	4419	65.28	463(24)		(5) $S_{sp}$ -ModHp16	243	53.58	6.7 (0.6)
	(3) $V_{mc}$ -WavDe162	6197	64.15	507(46)		(18) $S_p$ -WavLp160	195	51.99	6.5(0.6)
<b>3</b>	<b>(1) <math>S_{r1}</math>-GauDe1</b>	<b>197</b>	<b>75.70</b>	<b>39(1.6)</b>	<b>10</b>	<b>(1) <math>V_{vc}</math>-GauHp240</b>	<b>1191</b>	<b>74.59</b>	<b>103(4.9)</b>
	(8) $S_{fd}$ -ModHp7	180	76.09	35(1.9)		(51) $V_{vc}$ -ModLp14	728	71.29	71(6.1)
	(35) $S_{r1}$ -WavHp35	161	63.92	22(1.6)		(22) $PmoyPlis\_WavLp600$	830	75.29	98(6.2)
<b>4</b>	(10) $S_{pk}$ -GauLp300	1744	4.30		<b>11</b>	<b>(1) DensPlis_GauHp4</b>	<b>195</b>	<b>87.20</b>	<b>50.2(2)</b>
	<b>(1) <math>S_{vi}</math>-ModLp88</b>	<b>23963</b>	<b>5.75</b>			(23) $NbMotifs\_ModHp6$	163	86.37	53.3(3.4)
	(5) $S_{10z}$ -WavLp23	5383	4.60			(65) $DensPlis\_WavLp80$	150	85.55	45.4(3.0)
<b>5</b>	(4) $S_k$ -GauHp78	4561	85.02	500(95.4)	<b>12</b>	(2) $PmoyPlis\_GauLp14$	279	78.36	53(3.3)
	<b>(1) <math>S_k</math>-ModHp104</b>	<b>5974</b>	<b>83.07</b>	<b>447(92)</b>		<b>(1) Spc_ModLp19</b>	<b>340</b>	<b>74.94</b>	<b>56(5.0)</b>
	(75) $S_k$ -WavHp156	2525	74.66	236(69.6)		(9) $S_k$ -WavLp4	262	81.80	66(7.2)
<b>6</b>	(2) $S_{tr}$ -GauDe12	582	76.40	53(12)	<b>13</b>	(5) $S_{fd}$ -GauLp20	191	43.52	249(25)
	<b>(1) <math>S_{pc}</math>-ModLp325</b>	<b>661</b>	<b>72.30</b>	<b>51(10)</b>		<b>(1) DensPlis_ModLp40</b>	<b>643</b>	<b>43.77</b>	<b>178(33)</b>
	(18) $S_{tr}$ -WavHp325	164	78.00	46(14)		(3) $S_q$ -WavLp88	273	49.06	197(42)
<b>7</b>	<b>(1) <math>V_{mc}</math>-GauDe20</b>	<b>2718</b>	<b>60.40</b>	88(4.4)	<b>14</b>	(2) $S_{tr}$ -GauHp19	4801	16.30	
	(8) $V_{mc}$ -ModHp100	1468	52.60	104(7.4)		(13) $S_{tr}$ -ModHp400	1073	8.90	
	(9) $DensPlis\_WavDe600$	1314	49.00	34(2.4)		<b>(1) S10z_WavLp50</b>	<b>6724</b>	<b>6.20</b>	

Identifier information: Identifier information:



prosthesis), 6 (Hot mill rolling) 10 (roping) and 3 (Sand blasting). The first three processes are characterized by high anisotropy [55]. For example, in the case of experiment 9 (wear of prosthesis), generally scratches with widths less than 10  $\mu\text{m}$  present a high degree of anisotropy [48]. This is due to the lack of degree of articulation.

- The  $S_{sk}$  roughness parameter given by DWT, high pass filtering and an evaluation length under 16  $\mu\text{m}$  characterizes efficient wear in a prosthesis [56–58].
- For a periodic anisotropic structure such as experiment 8 (hard turning machining), wavelet analysis is shown to be inadequate, and the Gaussian technique is confirmed to be more appropriate [59].
- A commonly measured feature of 3D surface topography is anisotropy [60], contrasting with 2D topography [61]. However, only two standardized parameters ( $S_{tr}$  and  $S_{ai}$ ) quantify anisotropy [62,63]. Consequently Mezghani [40] has defined an anisotropic 3D complex wavelet that computes parameters related to DWT, even if the spatial resolution of multiscale analyses is invariant, as in this study, which contrasts the surface analyses presented in [64]. DWT used with the same factor of dilatation as if the structure were anisotropic yields a modulated anisotropy of the surface [65] but does not quantify the relevant scale [66]. This may explain the irrelevant results obtained with the wavelet approach to characterize anisotropic surfaces using the standardized parameters. A way to address this issue in the future should be to use 2D measurements in the appropriate isotropic direction [67]. The first results suggest that micro-scale 2D topography in the principal direction of anisotropy is more relevant than multiscale 3D topography [68]. This could explain why DWT gives relevant results for TP9, TP6 and TP13.
- Concerning others studies, DWT gives poor relevance compared to both other multiscale methods. In the case of polishing, DWT appears to perform poorly (TP3 and TP5); the  $F_{mean}$  relevance value decreases by a factor of two. This is due to the complexity and high fractal aspect of these surfaces [69]. For this type of surface, GF appears to be appropriate; this also explains why Weierstrass surfaces have been used to model engineering fractal surfaces [70], contact mechanics, wear and super-finishing abrasive process. Gaussian analyses are shown to better characterize complex ergodic fractal surfaces compared to the wavelet technique because the robustness of DWT is poor for a continuous spectrum, even if this technique is adapted to detect a particular signature in a complex topographical signal [71]. This is confirmed by the TP12 results (i.e., brushing super-finishing), from which DWT is shown to be relevant to determine the signature of the first stage of the sandblasting process even after other complex processes (i.e., brushing). This study illustrates that DWT quantifies prior process conditions. This feature of the DWT approach is well known in the field of mechanical engineering, including dynamics [72], seismic signal [73], and tool machining [74], but its relevance in topographical analysis map is still an object of discussion.

The results of this study concerning DWT confirm and reveal that this multiscale technique:

- is relevant to quantify localized defaults;
- is appropriate to isolate different complex signature, if they clearly differ;
- is appropriate to analyse classical anisotropic topographies, until more powerful roughness parameters are employed (currently not defined in the 3D standards);
- is irrelevant to describe complex tribological topographies.

### 5.1.2. Gaussian and Modal approaches

As some applications of DWT compared to GF have been discussed already, the following discussion focuses on the differences between the Gaussian and Modal approaches.

- Firstly, a high discrepancy of Modal analysis is noted for TP8 (high precision tool machining) and TP10 (plastic deformation). Experiment 8 concerns surfaces with highly periodical topographical components [75]. It is thus confirmed that such topographies are appropriate to be treated with GF. Basically, the modal decomposition basis gathers Gaussian decomposition (sine and cosine bases) to obtain an amplitude modulation with a tight frequency band. This explains why Gaussian analysis, which is based on periodical morphological structure, is appropriate for highly periodic signals.
- To describe more complex tribological processes, the DMD technique appears to give similar results as GF; such is the case for TP5 (belt finishing), TP2 (sand blasting), TP6 (hot mil rolling), TP8 (wear prosthesis) and TP12 (brushing). Currently, it remains difficult to explain modal analysis features in detail because the technique is still new and unfamiliar. A first explanation may be that a modal basis can be described in a Fourier basis in a more compact form [76] because the number of significant components described in this complex system can be described as a continuous spectrum (i.e., the  $1/f^\alpha$  spectrum), which is well known to describe complex physical morphological systems [77]. For tribological studies, a high number of complex systems can be described by this power law spectrum [78], such as contact mechanics, machined surfaces [79], tribological diffusion [80], diffusion in hot temperature [81], tool wear [82], cutting [83] or lubrication [84]. In the case of a continuous spectrum, each term of the modal basis can be reorganized to be equivalent to the Gaussian representation, and thus, all complex continuous spectra that exhibit a  $1/f^\alpha$  spectrum without a particular signature will lead to equivalent results in terms of modal or Gaussian analysis.
- However, for experiments that present localized components, the DMD technique clearly leads to better results than GF. This feature emerges particularly for the case of processes leading to pitting (TP14 and TP4).

The results concerning the DMD approach compared to other multiscale methods reveal that this technique:

- is more relevant in quantifying localized default (i.e., such as pitting) than the Gaussian technique but less relevant than DWT for this type of topography;
- is appropriate to characterize different complex tribological systems with a  $1/f$  spectra and is also equivalent to GF for such cases;
- is less appropriate than GF to describe purely periodic topographic components (e.g., turning process). For GF, the results compared to other multiscale methods confirm and reveal that this technique:
- is appropriate to characterize a purely (i.e., pseudo) periodical morphological structure;
- is appropriate to characterize different complex tribological system with a  $1/f$  spectra (i.e., equivalence with DMD analysis and highly superiority compared with DWT);
- is not appropriate to quantify localized geometric variations, which DWT or even modal analysis can characterize.

### 5.1.3. Relevance of multiscale approaches for 3D analysis

Diagram 6 illustrates the relevance of MA compared to conventional approaches. Before detailing this diagram, an important notion in topography functional analysis must be noted. For each 2D or 3D topographical analysis to compute roughness parameters, a first analysis should verify if the scale of observation is appropriate. For the authors, this clearly means that the physical phenomena can be observed on the measured topography. As an example, for tooled machining surfaces that present an apparent periodic motif, the engineer should try to record several grooves to ensure a good characterization and significant roughness parameters.

To consider scale, standards have defined that the widest motif to be analysed should be equivalent to  $1/5$  of the evaluation length (i.e., a generalization of Shannon principle). More precisely, the sampling length is the length on which the surface parameters are calculated (e.g., the cut-off length for a waviness or roughness profile, the total profile length for a raw profile). Parameters calculated from the sampling length are named assessed parameters (ISO 4288), and the final parameters values are computed from the assessed values average; 5 sampling lengths are preconized. As an example, an  $R_a$  value is obtained from the average of assessed values computed on each sampling length available in the profile: on a 12.5 mm measured profile analysed with a Gaussian cut-off of 0.8 mm, the filtered profile measure  $12.5 - 0.8 = 11.7$  mm (i.e., approximately 14 sampling lengths). This allows local variations to be averaged and ensure a stable and significant  $R_a$  value. For 3D measurements, no recommendation is currently proposed, and consequently, the scale of the tribological phenomena to be characterized by a roughness parameter lies under the sampling length. Thus, a multiscale approach must be performed to provide a significant characterization of roughness parameters. This necessity is confirmed in this study and illustrated in Fig. 6.

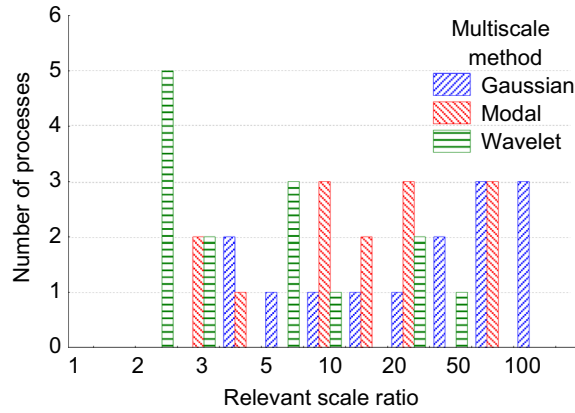


Fig. 6. Repartition of the relevant scale ratios.

For each tribological process, this graph shows that the relevance range lies from 3 to 100. Thus, based on a large collection of data, this study clearly confirms that multiscale analyses are required to analyse tribological topographic issues. This graph also clearly shows that a statistical method must be used to determine the most relevant spatial scale with respect to the tribological processes to be analysed. The MesRug<sup>TM</sup> expert system appears to be an appropriate tool to perform such statistical analysis and allows investigation of the relevant scales.

A perspective of this kind of approach should consist in applying the MA on the surface slopes and/or curvature mappings, as proposed in [85]. Indeed, curvature indicators often enable a better understanding of functional correlations.

## 6. Conclusions

This study presents a methodology for the comparison of three types of multiscale analyses, namely Discrete Wavelet Transform, Gaussian Transform and Discrete Modal Decomposition. The method is applied to different tribological processes, on which we have detailed the use of statistical indicators using the MesRug<sup>TM</sup> system and the effectiveness of the different steps of this new approach.

- (i) This study is built on a collection of large data sets enabling a non-oriented comparison of the 3 compared multiscale approaches.
- (ii) For each method, this study investigated the scale of the analysis, the type of filter (i.e., Low-pass, High-pass and bandpass) and the relevance of the existing 3D surface roughness parameters.
- (iii) This study clearly demonstrates the necessity of using a multiscale approach for tribological topographies analysis.
- (iv) It has been shown that the Wavelet approach is the most relevant to characterize localized surface defects, such as pitting.
- (v) It has been shown that the Gaussian approach is the most relevant to characterize highly periodical morphological structures.
- (vi) Both Modal decompositions and Gaussian transforms appear appropriate and have similar performance for high complexity structures.
- (vii) Finally, this study found that Modal Decomposition yields results that are effectively a compromise between the Gaussian and Wavelet approaches; the method is more relevant than the Gaussian method for localized defects, and less relevant for highly periodic structures. This can be explained by the modulated frequency/amplitude descriptors generated to decompose with a modal basis.

A synthesis of multiscale approaches features revealed through this multiscale methods comparison is presented in Table 6.

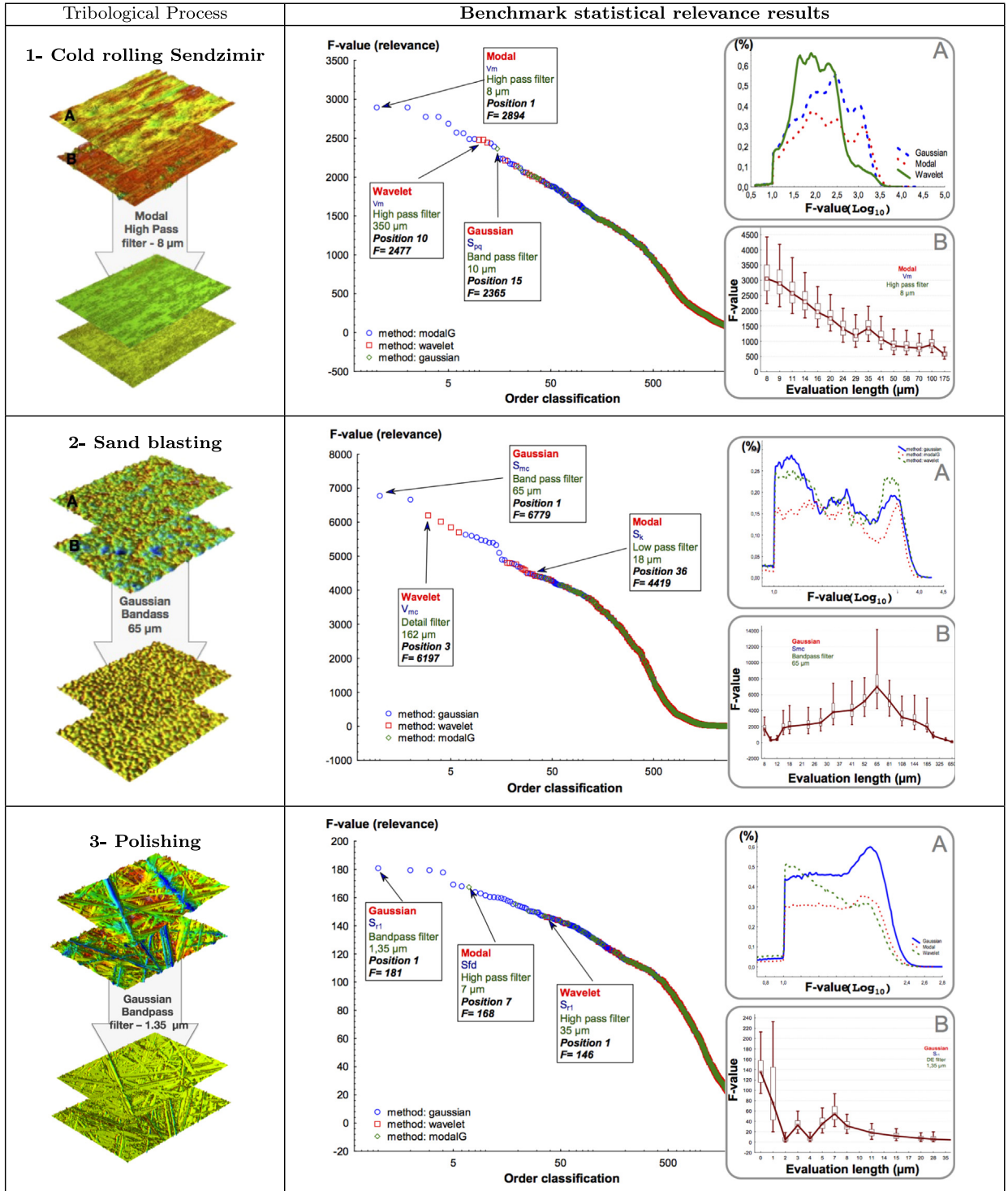
Table 6  
Multiscale methods features.

Characteristic of the topographical map	Wavelet	Modal	Gaussian
Aptitude to detect multiscale properties	++	+++	+++
Periodical or pseudo periodical structure (tool machining, etc.)	-	-	++
Complex morphological structure	-	++	++
Topographical signature in the complex signal (pitting, etc.)	+++	++	-
Aptitude to analyse anisotropic processes (grooves, etc.)	++	+	-

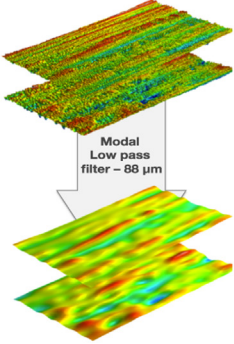
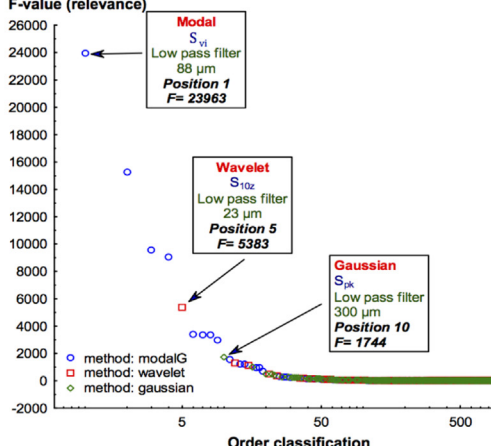
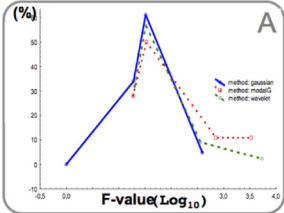
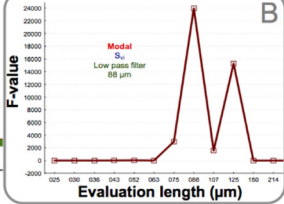
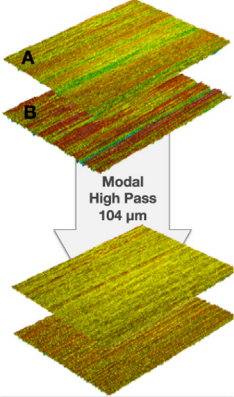
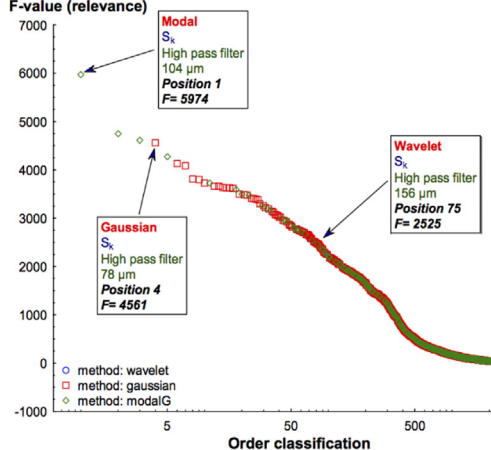
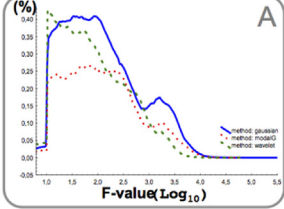
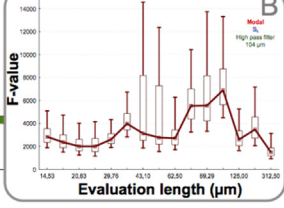
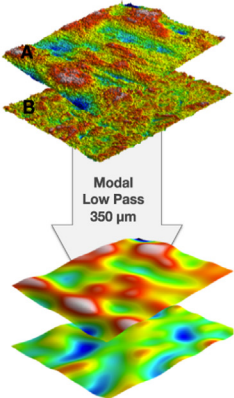
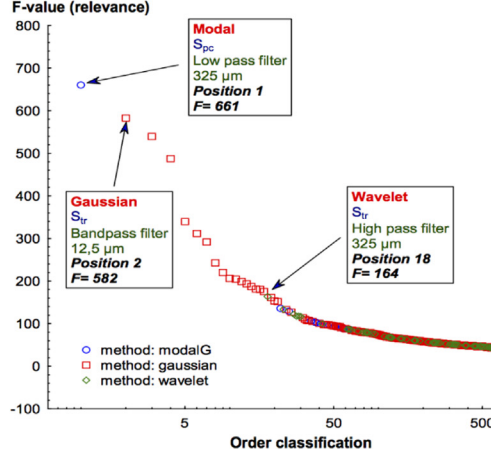
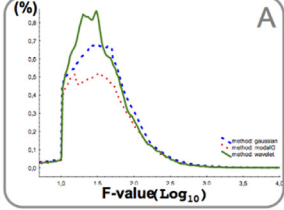
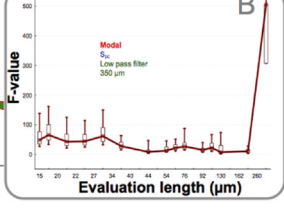
# Appendix A. Tables of results

See Tables A1–A5.

**Table A1**  
Relevance results for TP1-3.



**Table A2**  
Relevance results for TP4-6.

Tribological Process	Benchmark statistical relevance results
<p><b>4- Bi-disk tribometer</b></p>  <p>Modal Low pass filter – 88 μm</p>	<p><b>F-value (relevance)</b></p>  <p> <b>Modal</b>  <math>S_{vj}</math>          Low pass filter          88 μm  <b>Position 1</b>  <b>F= 23963</b> </p> <p> <b>Wavelet</b>  <math>S_{10z}</math>          Low pass filter          23 μm  <b>Position 5</b>  <b>F= 5383</b> </p> <p> <b>Gaussian</b>  <math>S_{pk}</math>          Low pass filter          300 μm  <b>Position 10</b>  <b>F= 1744</b> </p> <p>         ○ method: modalG          □ method: wavelet          ◇ method: gaussian     </p> <p><b>F-value (%)</b></p>  <p><b>A</b></p> <p><b>F-value (%)</b></p>  <p><b>B</b></p> <p><b>F-value</b></p> <p><b>Evaluation length (μm)</b></p>
<p><b>5- Belt finishing</b></p>  <p>Modal High Pass 104 μm</p>	<p><b>F-value (relevance)</b></p>  <p> <b>Modal</b>  <math>S_{vj}</math>          High pass filter          104 μm  <b>Position 1</b>  <b>F= 5974</b> </p> <p> <b>Gaussian</b>  <math>S_x</math>          High pass filter          78 μm  <b>Position 4</b>  <b>F= 4561</b> </p> <p> <b>Wavelet</b>  <math>S_x</math>          High pass filter          156 μm  <b>Position 75</b>  <b>F= 2525</b> </p> <p>         ○ method: wavelet          □ method: gaussian          ◇ method: modalG     </p> <p><b>F-value (%)</b></p>  <p><b>A</b></p> <p><b>F-value (%)</b></p>  <p><b>B</b></p> <p><b>F-value</b></p> <p><b>Evaluation length (μm)</b></p>
<p><b>6- Hot mill rolling</b></p>  <p>Modal Low Pass 350 μm</p>	<p><b>F-value (relevance)</b></p>  <p> <b>Modal</b>  <math>S_{pc}</math>          Low pass filter          325 μm  <b>Position 1</b>  <b>F= 661</b> </p> <p> <b>Gaussian</b>  <math>S_r</math>          Bandpass filter          12,5 μm  <b>Position 2</b>  <b>F= 582</b> </p> <p> <b>Wavelet</b>  <math>S_r</math>          High pass filter          325 μm  <b>Position 18</b>  <b>F= 164</b> </p> <p>         ○ method: modalG          □ method: gaussian          ◇ method: wavelet     </p> <p><b>F-value (%)</b></p>  <p><b>A</b></p> <p><b>F-value (%)</b></p>  <p><b>B</b></p> <p><b>F-value</b></p> <p><b>Evaluation length (μm)</b></p>



**Table A3**  
Relevance results for TP7-9.

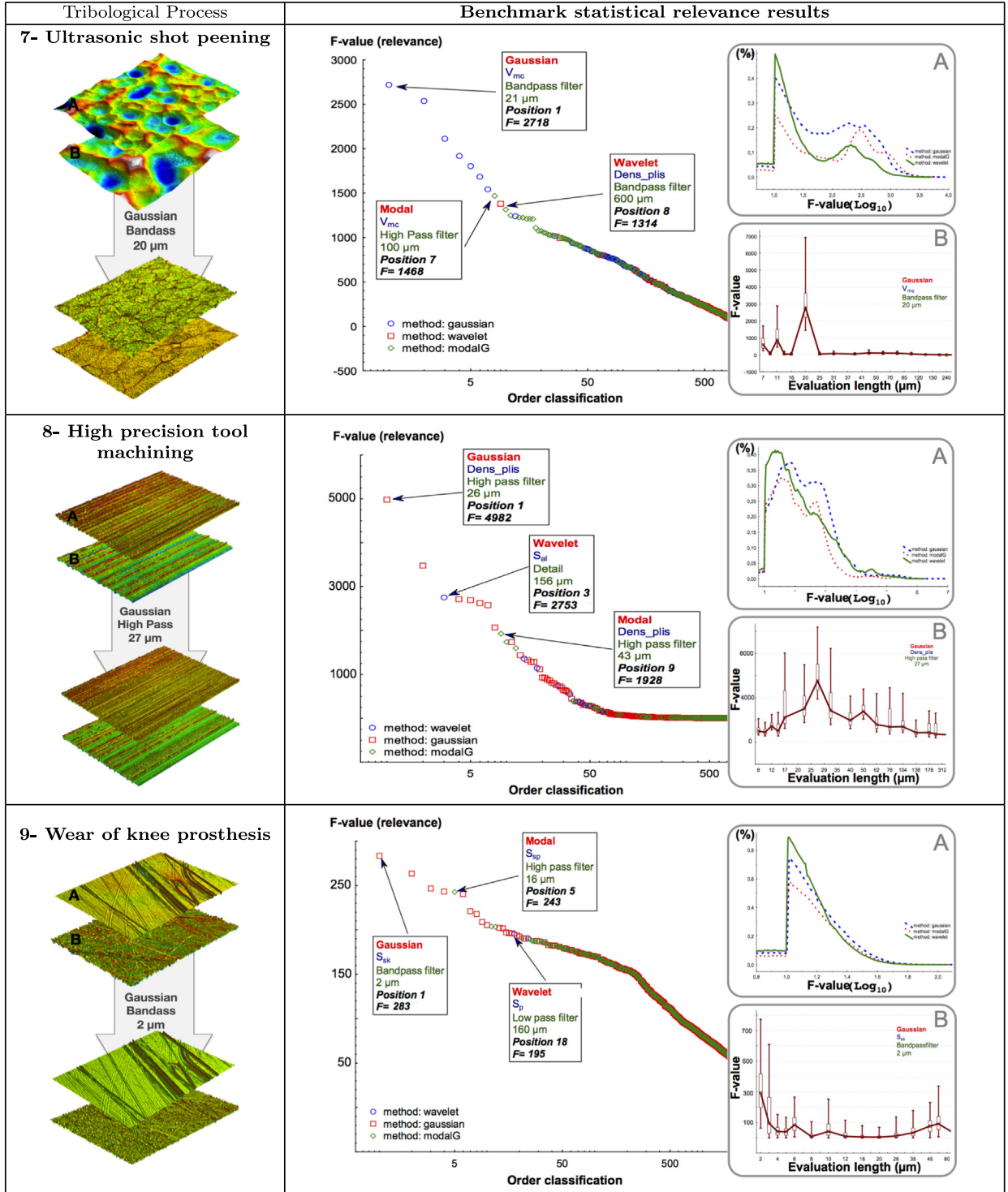


**Table A4**  
Relevance results for TP10-12.

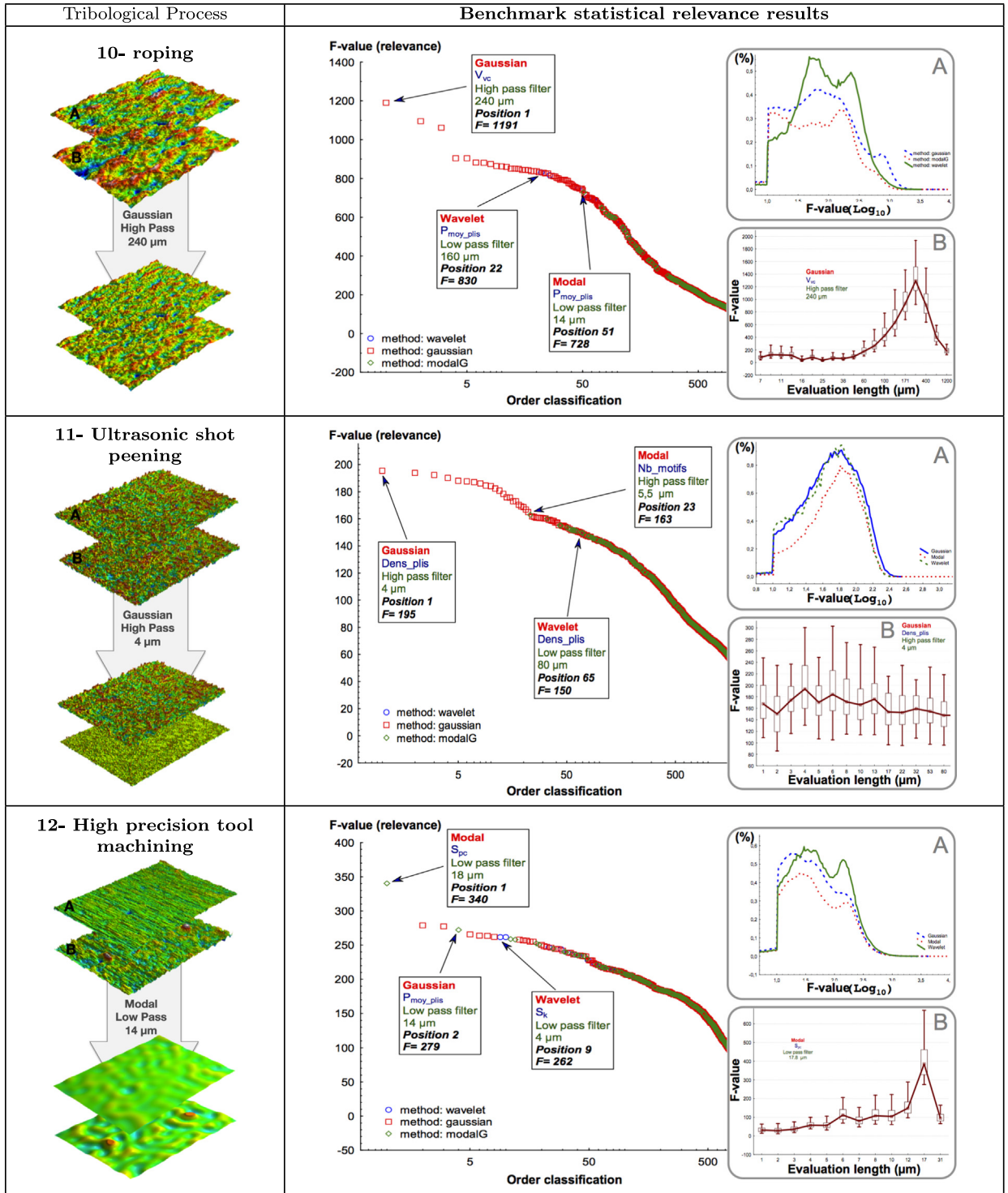
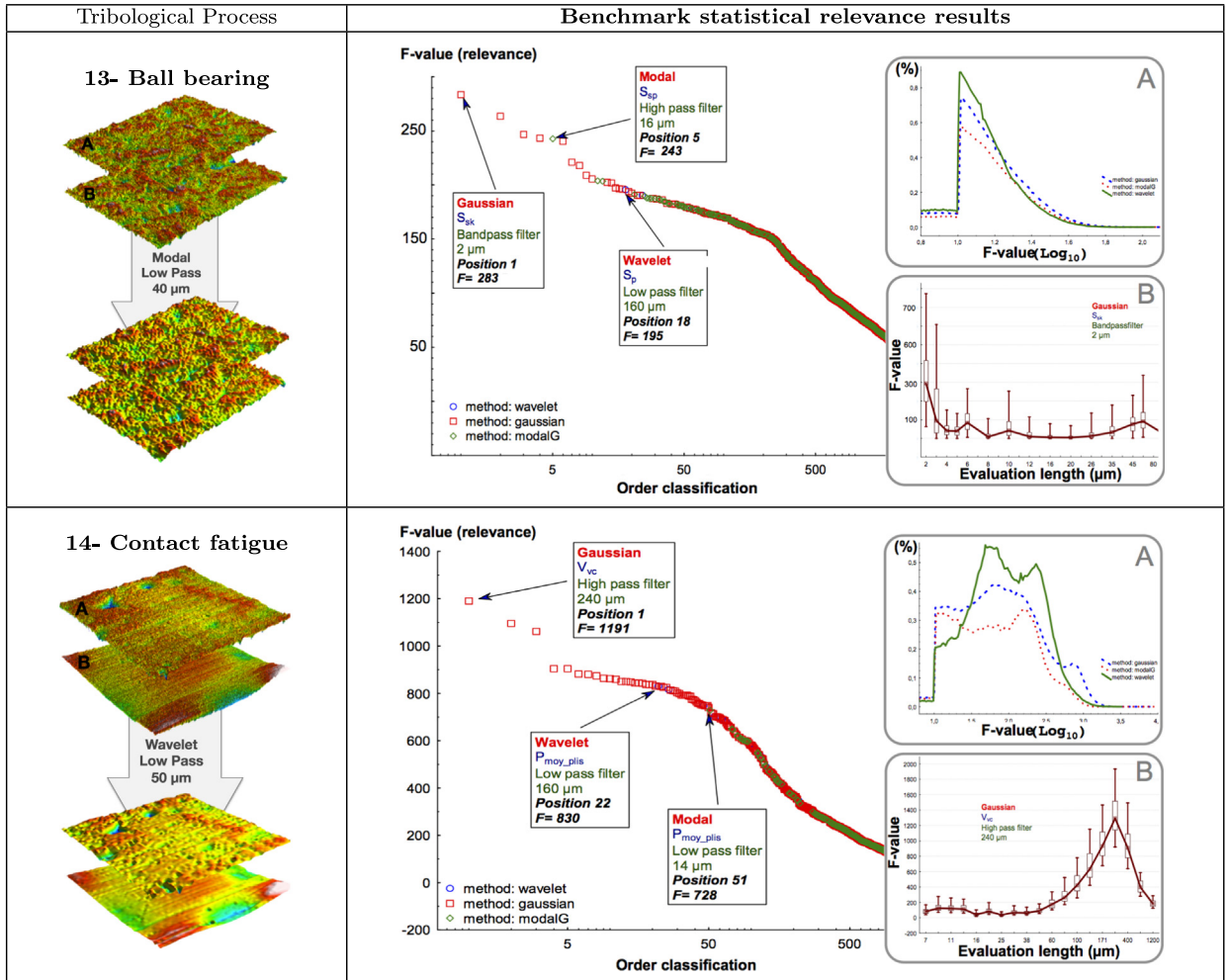


**Table A5**  
Relevance results for TP13-14.



## Appendix B. Main nomenclature and abbreviation

See [Table B1](#).

**Table B1**  
Nomenclature and abbreviations.

Nomenclature		
Name	Description	
Process	This term is used in this paper in the sense of "continuous series of actions meant to accomplish some result". The processes considered are finishing processes (sand blating, polishing, belt finishing, bi-disk tribometry, ultrasonic shot penning, brushing), metal forming (hot mill rolling), or machining processes (precision hard turning). Other tribological phenomena are also abusively referred as "processes" (wear, roping, ball bearing conditions, effect of lubricant in a gear...)	
Multiscale roughness analysis	A multiscale roughness analysis consists in analysing the roughness topography of a surface at different spatial scales, generally by applying to a 3D cloud of measured points a multiscale decomposition. The aim is generally to make emerge the relevant scale(s) to observe/analyse a surface measurement	
Roughness functional analysis	Roughness functional analysis means that the surface roughness is analysed with the aim of investigating the correlations between the surface measurement (or an indicator extracted from the measured 3D cloud of points) and a specified function or behaviour of the surface	
Abbreviations		
Multiscale methods	Description	References
DCT	Discrete Cosine Transform. The discrete cosine transform method is a decomposition that performs a projection in a geometric vectorial basis composed with cosine functions at different frequencies. A linear combination of these geometric elements is thus obtained. This method is often used in image processing for data compression	[41,86,87]
GF	Gaussian Filtering. The Gaussian filter consists in a continuous convolution that use the Gaussian 2D or 3D shape as weight function. This technique is standardized (ISO and ASME), where precognized cut-offs for high pass and low pass filtering are specified	[3,19,31–33]
DWT	Discrete Wavelet Transform. A wavelet transform decomposes the measured 3D surface into basis functions composed of wavelets. The calculation is performed at different scales of observation (multi-resolution). Discrete wavelet transform means that the wavelets used to make the transformation are discretely sampled	[20,34–40]
DMD	Discrete Modal Decomposition. A Discrete Modal Decomposition decomposes a signal within a spectral basis built from eigenmodes, by projecting the measured surface into an eigen-basis built from structural dynamics. This eigen-basis is defined by its eigenvectors, called modal vectors.	[5,30,42,43]
Hardware & software	Description	
WLI	White Light Interferometry (roughness measurement technology)	
MesRug™	MesRug™ is a statistical expert system that enables the classification of roughness parameters according to the surface functionality considered, by computing statistical relevance indicators. In this manner, results of roughness experimental designs (DOE) can be visualized and examined to reveal robustly the relevant scale(s) and surface parameter(s) with respect to a surface function	
Others	Description	
MA	Multi-scale analysis	
TP	Tribological Process	
UHMWPE	Ultra-High Molecular Weight Poly-ethylene (type of knee prosthesis)	
PHT	Precision Hard Turning (machining technique)	

## References

- [1] ISO 4287, Geometrical Product Specifications (GPS)—Surface texture: Profile method—Terms, Definitions and Surface Texture Parameters, 1997.
- [2] ISO 13565-1, Geometrical Product Specifications (GPS)—Surface Texture: Profile method; Surfaces Having Stratified Functional Properties—Part 1: Filtering and General Measurement Conditions, 1996.
- [3] ASME B46.1, Surface Texture—Surface Roughness, Waviness and Lay—American National Standard, 2009.
- [4] ISO 25178-2, Geometrical Product Specifications (GPS)—Surface Texture: Areal—Part 2: Terms, Definitions and Surface Texture Parameters, 2012.
- [5] J. Grandjean, G. le Goic, H. Favreliere, Y. Ledoux, S. Samper, F. Formosa, L. Devun, T. Gradel, Multi-scalar analysis of hip implant components using modal decomposition, *Meas. Sci. Technol.* 23 (12) (2012) 125702.
- [6] W.L. Walter, S.M. Kurtz, C. Eposito, W. Hozack, K.G. Holley, J.P. Garino, M.A. Tuke, Retrieval analysis of squeaking alumina ceramic-on-ceramic bearings, *Br. J. Bone Joint Surg.* 93 (12) (2011) 1597–1601.
- [7] F.W. Chan, J.D. Boby, J.B. Medley, J.J. Krygier, M. Tanzer, Wear and lubrication of metal-on-metal hip implants, *Clin. Orthop. Relat. Res.* 369 (1999) 10–24.
- [8] S.C. Scholes, A. Unsworth, Comparison of friction and lubrication of different hip prostheses, *Proc. Inst. Mech. Eng. Part H: J. Eng. Med.* 214 (H1) (2000) 49–57.
- [9] M.T. Bengisu, A. Akay, Stick-slip oscillations: dynamics of friction and surface roughness, *J. Acoust. Soc. Am.* 105 (1) (1999) 194–205.
- [10] A. Soom, J.W. Chen, Simulation of random surface roughness-induced contact vibrations at Hertzian contacts during steady sliding, *J. Tribol.* 108 (1) (1986) 123–127.

- [11] D.J. Thompson, Wheel-rail noise generation, Part I: introduction and interaction model, *J. Sound Vib.* 161 (3) (1993) 387–400.
- [12] Y.T. Su, M.H. Lin, M.S. Lee, The effects of surface irregularities on roller bearing vibrations, *J. Sound Vib.* 165 (3) (1993) 455–466.
- [13] R.S. Sayles, S.Y. Poon, Surface topography and rolling element vibration, *Precis. Eng.* 3 (3) (1981) 137–144.
- [14] G.G. Gray, K.L. Johnson, The dynamic response of elastic bodies in rolling contact to random roughness of their surfaces, *J. Sound Vib.* 22 (3) (1972) 323–342.
- [15] Q. Wang, Z. Jiang, J. Zhao, M. Fang, Multi-factor coupling system characteristic of the dynamic roll gap in the high-speed rolling mill during the unsteady lubrication process, *Tribol. Int.* 67 (3) (2013) 174–181.
- [16] K.A. Risbood, U.S. Dixit, A.D. Sahasrabudhe, Prediction of surface roughness and dimensional deviation by measuring cutting forces and vibrations in turning process, *J. Mater. Process. Technol.* 132 (1–3) (2003) 203–214.
- [17] D.Y. Jang, Y.G. Choi, H.G. Kim, A. Hsiao, Study of the correlation between surface roughness and cutting vibrations to develop an on-line roughness measuring technique in hard turning, *Int. J. Mach. Tools Manuf.* 36 (3) (1996) 453–464.
- [18] O.B. Abouelatta, J. Madl, Surface roughness prediction based on cutting parameters and tool vibrations in turning operations, *J. Mater. Process. Technol.* 118 (1–3) (2001) 269–277.
- [19] J. Raja, B. Muralikrishnan, Recent advances in separation of roughness, waviness and form, *Precis. Eng.* (3) (2002) 222–235.
- [20] X. Chen, J. Raja, S. Simanapalli, Multi-scale analysis of engineering surfaces, *Int. J. Mach. Tools Manuf.* 35 (2) (1995) 231–238.
- [21] J. Berglund, C. Agunwamba, B. Powers, C.A. Brown, B.G. Rosèn, On discovering relevant scales in surface roughness measurement—an evaluation of a band-pass method, *Scanning* 32 (4) (2010) 244–249.
- [22] M. Bigerelle, T. Mathia, S. Bouvier, The multi-scale roughness analyses and modeling of abrasion with the grit size effect on ground surfaces, *Wear* 286–287 (2012) 124–135.
- [23] J. Berglund, C.A. Brown, B.G. Rosèn, N. Bay, Milled die steel surface roughness correlation with steel sheet friction, *CIRP Ann.—Manuf. Technol.* 59 (1) (2010) 577–580.
- [24] L. de Chiffre, P. Leonardo, H. Trumpold, D.A. Lucca, G. Goch, C.A. Brown, J. Raja, H.N. Hansen, Quantitative characterisation of surface texture, *CIRP Ann.—Manuf. Technol.* (2000) 635–652.
- [25] C.A. Brown, W.A. Johnsen, R.M. Butland, Scale-sensitive fractal analysis of turned surfaces, *CIRP Ann.—Manuf. Technol.* (1996) 515–518.
- [26] S.E. Jordan, C.A. Brown, Comparing texture characterization parameters on their ability to differentiate ground polyethylene ski bases, *Wear* 261 (2006) 398–409.
- [27] S. Mezghani, H. Zahouani, Characterisation of the 3D waviness and roughness motifs, *Wear* 257 (12) (2004) 1250–1256.
- [28] A. Aubert, D. Jeulin, R. Hashimoto, Surface texture classification from morphological transformations, *Comput. Imaging Vis.* 18 (2000) 253–262.
- [29] ISO TS 16610-40, Geometrical Product Specifications (GPS)—Filtration—Part 40: Morphological Profile Filters: Basic Concepts, 2006.
- [30] S. Samper, F. Formosa, Form defects tolerancing by natural modes analysis, *J. Comput. Inf. Sci. Eng.* (2007) 44–51.
- [31] J. Raja, V. Radhakrishnan, Analysis and synthesis of surfaces profiles using fourier series, *Int. J. Mach. Tool Des. Res.* 17 (1977) 245–251.
- [32] Z. Peng, T.B. Kirk, Two-dimensional fast fourier transform and power spectrum for wear particle analysis, *Tribol. Int.* 30 (1997) 583–590.
- [33] ISO 12781-2, Geometrical Product Specifications (GPS)—Flatness—Part 2: Specification Operators, 2011.
- [34] S.G. Mallat, A theory for multiresolution signal decomposition: the wavelet representation, *IEEE Trans. Pattern Anal. Mach. Intell.* 11 (7) (1989) 674–693.
- [35] K. Lingadurai, M.S. Shunmugam, Metrological characteristics of wavelet filter used for engineering surfaces, *Measurement* 39 (7) (2006) 575–584.
- [36] Q. Chen, S. Yang, Surface roughness evaluation by using wavelets analysis, *Precis. Eng.* (1999) 209–212.
- [37] S.H. Lee, H. Zahouani, R. Caterini, T. Mathia, Morphological characterisation of engineered surfaces by wavelet transform, *Int. J. Mach. Tools Manuf.* 38 (5–6) (1998) 581–589.
- [38] L. Rosenboom, T. Kreis, W. Jüptner, Surface description and defect detection by wavelet analysis, *Meas. Sci. Technol.* (2011) 045102.
- [39] B. Josso, D.R. Burton, M.J. Lalor, Frequency normalised wavelet transform for surface roughness analysis and characterisation, *Wear* (2002) 491–500.
- [40] S. Mezghani, H. Zahouani, J. Piezanowski, Multiscale characterizations of painted surface appearance by continuous wavelet transform, *J. Mater. Process. Technol.* 211 (2) (2011) 205–211.
- [41] J. Lecompte, O. Legoff, J.Y. Hascoet, Technological form defects identification using discrete cosine transform method, *Int. J. Adv. Manuf. Technol.* 51 (9–12) (2010) 1033–1044.
- [42] H. Favreliere, Modal tolerancing: from metrology to specifications (Ph.D. thesis). Université de Savoie, France, 2009.
- [43] G. le Goic, H. Favreliere, S. Samper, F. Formosa, Multi scale modal decomposition of primary form, waviness and roughness of surfaces, *Scanning, The Journal of Scanning Microscopies* 33 (2011) 332–341. (Special Issue on Surface Metrology II).
- [44] F. Barré, J. Lopez, Watershed lines and catchment basins: a new 3D-motif method, *Int. J. Mach. Tools Manuf.* 40 (8) (2000) 1171–1184.
- [45] A. Van Gorp, M. Bigerelle, M. El Mansori, P. Ghidossi, A. Iost, Effects of working parameters on the surface roughness in belt grinding process: the size-scale estimation influence, *Int. J. Mater. Prod. Technol.* 38 (1) (2010) 16–34.
- [46] K. Anselme, M. Bigerelle, Topography effects of pure titanium substrates on human osteoblast long-term adhesion, *Acta Biomater.* 1 (2) (2005) 211–222.
- [47] A. Van Gorp, M. Bigerelle, A. Grellier, A. Iost, D. Najjar, A multi-scale approach of roughness measurements: evaluation of the relevant scale, *Mater. Sci. Eng. C—Biomim. Supramol. Syst.* 27 (58) (2007) 1434–1438.
- [48] D. Najjar, M. Bigerelle, H. Migaud, A. Iost, About the relevance of roughness parameters used for characterizing worn femoral heads, *Tribol. Int.* 39 (12) (2006) 1527–1537.
- [49] S. Mezghani, L. Sabri, M. El Mansori, H. Zahouani, On the optimal choice of wavelet function for multiscale honed surface characterization, *J. Phys.: Conf. Ser.* 311 (2011) 012025.
- [50] H. Zahouani, S. Mezghani, R. Vargiolu, M. Dursapt, Identification of manufacturing signature by 2D wavelet decomposition, *Wear* (2008) 480–485.
- [51] M. Šraml, J. Flašker, Computational approach to contact fatigue damage initiation analysis of gear teeth flanks, *Int. J. Adv. Manuf. Technol.* 31 (11–12) (2006) 1066–1075.
- [52] J. Jiang, M.M. Stack, A. Neville, Modelling the tribo-corrosion interaction in aqueous sliding conditions, *Tribol. Int.* 35 (10) (2002) 669–679.
- [53] D. Najjar, M. Bigerelle, C. Lefebvre, A. Iost, A new approach to predict the pit depth extreme value of a localized corrosion process, *ISIJ Int.* 43 (5) (2003) 720–725.
- [54] M. Bigerelle, D. Najjar, T. Mathia, A. Iost, T. Coorevits, K. Anselme, An expert system to characterise the surfaces morphological properties according to their tribological functionalities: the relevance of a pair of roughness parameters, *Tribol. Int.* 59 (2013) 190–202.
- [55] D. Najjar, M. Bigerelle, H. Migaud, A. Iost, Identification of scratch mechanisms on a retrieved metallic femoral head, *Wear* 258 (14) (2005) 240–250.
- [56] R.M. Hall, P. Siney, A. Unsworth, The effect of surface topography of retrieved femoral heads on the wear of UHMWPE sockets, *Med. Eng. Phys.* 19 (8) (1997) 711–719.
- [57] S. Affatato, G. Bersaglia, Y. Junqiang, F. Traina, A. Toni, M. Viceconti, The predictive power of surface profile parameters on the amount of wear measured in vitro on metal-on-polyethylene artificial hip joints, *Proc. Inst. Mech. Eng. Part H: J. Eng. Med.* 220 (3) (2006) 457–464.
- [58] T.J. Joyce, H. Grigg, D.J. Langton, A. Nargol, Quantification of self-polishing in vivo from explanted metal-on-metal total hip replacements, *Tribol. Int.* 44 (5) (2011) 513–516.
- [59] S.M. Pandit, M.C. Shaw, Characteristic shapes and wavelength decomposition of surfaces in machining, *CIRP Ann.—Manuf. Technol.* 30 (1) (1981) 487–492.
- [60] K.J. Stout, L. Blunt, W.P. Dong, E. Mainsah, N. Luo, T. Mathia, P.J. Sullivan, H. Zahouani, Development of Methods for the Characterisation of Roughness in three Dimensions, European Report EUR 15178N, 2000, pp. 1–384.

- [61] W.P. Dong, P.J. Sullivan, K.J. Stout, Comprehensive study of parameters for characterising three-dimensional surface topography: III: parameters for characterising amplitude and some functional properties, *Wear* (1994) 29–43.
- [62] P. Pawlus, L. Galda, A. Dzierwa, W. Koszela, Abrasive wear resistance of textured steel rings, *Wear* (2009) 1873–1882.
- [63] L. Blunt, S. Ebdon, The application of three-dimensional surface measurement techniques to characterizing grinding wheel topography, *Int. J. Mach. Tools Manuf.* (1996) 1207–1226.
- [64] S. Mezghani, H. Zahouani, J. Piezanowski, Multiscale effect of paint pulverization orientation on appearance after painting, *J. Phys.: Conf. Ser.* 311 (2011) 012026.
- [65] A. Arneodo, N. Decoster, S.G. Roux, A wavelet-based method for multifractal image analysis. I. Methodology and test applications on isotropic and anisotropic random rough surfaces, *Eur. Phys. J. B—Condens. Matter Complex Syst.* 15 (3) (2000) 567–600.
- [66] S.G. Roux, A. Arneodo, N. Decoster, A wavelet-based method for multifractal image analysis. III. Applications to high-resolution satellite images of cloud structure, *Eur. Phys. J. B* 15 (4) (2000) 765–786.
- [67] T. Mathia, P. Pawlus, Recent trends in surface metrology, *Wear* (2010) 494–508.
- [68] M. Bigerelle, A. Van Gorp, A. Iost, Multiscale roughness analysis in injection—molding process, *Polym. Eng. Sci.* (2008) 1725–1736.
- [69] M.D. Costa, M. Bigerelle, D. Najjar, A new methodology for quantifying the multi-scale similarity of images, *Microelectron. Eng.* (2007) 424–430.
- [70] A. Majumdar, C.L. Tien, Fractal characterization and simulation of rough surfaces, *Wear* 136 (2) (1990) 313–327.
- [71] M. El Mansori, S. Mezghani, L. Sabri, H. Zahouani, On concept of process signature in analysis of multistage surface formation, *Surf. Eng.* 26 (3) (2010) 216–223.
- [72] H. Qiu, J. Lee, J. Lin, G. Yu, Wavelet filter-based weak signature detection method and its application on rolling element bearing prognostics, *J. Sound Vib.* 289 (4–5) (2006) 1066–1090.
- [73] P. Goupillaud, A. Grossmann, J. Morlet, Cycle-octave and related transforms in seismic signal analysis, *Geoexploration* (1984) 85–102.
- [74] K. Zhu, Y.S. Wong, G.S. Hong, Wavelet analysis of sensor signals for tool condition monitoring: a review and some new results, *Int. J. Mach. Tools Manuf.* 49 (78) (2009) 537–553.
- [75] C. Daniel, F. Mücklich, Z. Liu, Periodical micro-nano-structuring of metallic surfaces by interfering laser beams, *Appl. Surf. Sci.* (2003) 317–321.
- [76] F.J. Fahy, Statistical energy analysis: a critical overview, *Philos. Trans. R. Soc. A: Math. Phys. Eng. Sci.* 346 (1681) (1994) 431–447.
- [77] T. Antal, M. Droz, G. Györgyi, Z. Rácz, Roughness distributions for  $1/\alpha$  signals, *Phys. Rev. E* (2002) 046140.
- [78] F.F. Ling, Fractals, engineering surfaces and tribology, *Wear* (1990) 141–156.
- [79] K. Wang, C.X. Yang, X.G. Yuan, Evaluation of the wavelet transform method for machined surface topography I: methodology validation, *Tribol. Int.* 36 (7) (2003) 517–526.
- [80] M. Schargott, V. Popov, Diffusion as a model of formation and development of surface topography, *Tribol. Int.* (2006) 431–436.
- [81] M. Bigerelle, J. Favregeon, T. Mathia, A. Iost, Multiscale modelling of morphological evolution of rough surface during superficial, volume and evaporation-condensation diffusions, *Defect Diffus. Forum* 323–325 (2012) 101–107.
- [82] P. Pfeifer, Fractal dimension as working tool for surface-roughness problems, *Appl. Surf. Sci.* 18 (1–2) (1984) 146–164.
- [83] D.R. Salgado, F.J. Alonso, I. Cambero, A. Marcelo, In-process surface roughness prediction system using cutting vibrations in turning, *Int. J. Adv. Manuf. Technol.* 43 (1–2) (2008) 40–51.
- [84] J. Michalski, Surface topography of the cylindrical gear tooth flanks after machining, *Int. J. Adv. Manuf. Technol.* 43 (5–6) (2008) 513–528.
- [85] M. Vulliez, M.A. Gleason, A. Souto-Lebel, Y. Quinsat, C. Lartigue, S.P. Kordell, A.C. Lemoine, C.A. Brown, Multi-scale curvature analysis and correlations with the fatigue limit on steel surfaces after milling, *Proc. CIRP* 13 (2014) 308–313.
- [86] S.A. Khayam, The Discrete Cosine Transform: Theory and Application, Technical Report, Department of Electrical & Computer Engineering, Michigan State University, 2003.
- [87] W. Huang, D.A. Ceglarek, Mode-based decomposition of part form error by discrete-cosine-transform with implementation to assembly and stamping system with compliant parts, *CIRP Ann.—Manuf. Technol.* 51 (1) (2002) 21–26.